Observation of Temperature-Induced Crossover to an Orbital-Selective Mott Phase in $A_xFe_{2-y}Se_2$ (A = K, Rb) Superconductors

M. Yi,[1,2] D. H. Lu,[3] R. Yu,[4] S. C. Riggs,[1,2] J.-H. Chu,[1,2] B. Lv,[5] Z. K. Liu,[1,2] M. Lu,[1,6] Y.-T. Cui,[1] M. Hashimoto,[3] S.-K. Mo,[7] Z. Hussain,[7] C. W. Chu,[5] I. R. Fisher,[1,2] Q. Si,[4] and Z.-X. Shen[1,2]

[1]*Stanford Institute of Materials and Energy Sciences, Stanford University, Stanford, California 94305, USA*
[2]*Departments of Physics and Applied Physics, and Geballe Laboratory for Advanced Materials, Stanford University, Stanford, California 94305, USA*
[3]*Stanford Synchrotron Radiation Lightsource, SLAC National Accelerator Laboratory, Menlo Park, California 94025, USA*
[4]*Department of Physics and Astronomy, Rice University, Houston, Texas 77005, USA*
[5]*Department of Physics, Texas Center for Superconductivity, University of Houston, Houston, Texas 77204, USA*
[6]*National Laboratory of Solid-State Microstructures and Department of Materials Science and Engineering, Nanjing University, Nanjing 210093, China*
[7]*Advanced Light Source, Lawrence Berkeley National Lab, Berkeley, California 94720, USA*

(Received 1 September 2012; published 5 February 2013)

Using angle-resolved photoemission spectroscopy, we observe the low-temperature state of the $A_xFe_{2-y}Se_2$ (A = K, Rb) superconductors to exhibit an orbital-dependent renormalization of the bands near the Fermi level—the d_{xy} bands heavily renormalized compared to the d_{xz}/d_{yz} bands. Upon raising the temperature to above 150 K, the system evolves into a state in which the d_{xy} bands have depleted spectral weight while the d_{xz}/d_{yz} bands remain metallic. Combined with theoretical calculations, our observations can be consistently understood as a temperature-induced crossover from a metallic state at low temperatures to an orbital-selective Mott phase at high temperatures. Moreover, the fact that the superconducting state of $A_xFe_{2-y}Se_2$ is near the boundary of such an orbital-selective Mott phase constrains the system to have sufficiently strong on-site Coulomb interactions and Hund's coupling, highlighting the nontrivial role of electron correlation in this family of iron-based superconductors.

DOI: 10.1103/PhysRevLett.110.067003 PACS numbers: 74.70.Xa, 71.30.+h, 74.25.Jb, 79.60.−i

Electron correlation remains a central focus in the study of high-temperature superconductors. The strongly correlated cuprate superconductors are understood as doped Mott insulators (MI) [1], while the iron-based superconductors (FeSCs) have been found to be moderately correlated [2–4]. While the different FeSC families share the common Fe 3d low energy electronic structure, they vary in physical properties such as ordered magnetic moment and effective mass [5]. Electron correlation systematically varies from weak to moderate from the phosphides to the arsenides and to the Fe(Te,Se) chalcogenides, where heavy band renormalization [6,7] and polaronic behaviors [8] have been observed. However, even in the Fe(Te,Se) family, resistivity remains metallic [9]. The newest chalcogenide superconductors, $A_xFe_{2-y}Se_2$ (A = alkali metal) [10–14] (AFS), with a large moment of $3.3\mu_B$ [15], is the first FeSC family to exhibit insulating behavior in its phase diagram, which may suggest stronger correlation for certain doping regime.

Another important factor for understanding the FeSCs is their multiorbital nature. In such a system, orbital-dependent behavior as well as competition between inter- and intraorbital interactions could play a critical role in determining their physical properties. Theoretical models have considered correlation effects in the bad metal regime in terms of an incipient Mott picture [5,16–18], and the proximity to the Mott transition may be orbital dependent even for orbitally independent Coulomb interactions [19,20]. What arises from the model is an orbital-selective Mott phase (OSMP), in which some orbitals are Mott localized while others remain itinerant. First introduced in the context of the $Ca_{2-x}Sr_xRuO_4$ system [21], an OSMP may result from both the orbital-dependent kinetic energy and the combined effects of the Hund's coupling and crystal level splittings [22,23]. An OSMP links naturally with models of coexisting itinerant and localized electrons that have been proposed to compensate for the shortcomings of both strong coupling and weak coupling approaches [24,25]. However, to date, there has been no experimental evidence for OSMP in any FeSC.

In this Letter, we present angle-resolved photoemission spectroscopy (ARPES) data from two superconducting AFSs, $K_xFe_{2-y}Se_2$ (KFS), and $Rb_xFe_{2-y}Se_2$ (RFS), with T_C of 32 and 31 K, respectively, as well as insulating and intermediate AFSs (see Supplemental Material [26]). We observe the superconducting AFSs undergoing a temperature-induced crossover from a metallic state in which all three t_{2g} orbitals (d_{xy}, d_{xz} and d_{yz}) are present near the Fermi level (E_F) to a state in which the d_{xy} bands have diminished spectral weight while the d_{xz}/d_{yz} bands remain metallic. In addition, the intermediate doping shows stronger correlation than the superconducting

doping, as seen in the further renormalization of the d_{xz}/d_{yz} bands and the much more suppressed d_{xy} intensity, while the insulating doping has no spectral weight near E_F in any orbitals. From comparison with our theoretical calculations, our observations are most consistent with the understanding that the presence of strong Coulomb interactions and Hund's coupling place the superconducting AFSs near an OSMP at low temperatures and cross over into the OSMP at high temperatures, while the intermediate and insulating compounds are on the boundary of the OSMP and in the MI phase, respectively, suggesting the importance of electron correlation in this family of FeSCs.

The low-temperature electronic structure of KFS is shown in Fig. 1. The Fermi surface (FS) of KFS consists of large electron pockets at the Brillouin zone (BZ) corner—X-point—and a small electron pocket at the BZ center—Γ-point [Fig. 1(a)], consistent with previous ARPES reports [27–29]. For the crystallographic 2-Fe unit cell, local-density approximation (LDA) calculations predict two electron bands at X [30] [Fig. 1(i)]. While the FS map appears to show only one pocket at X, measurements under different polarizations [Figs. 1(j)–1(l)] reveal the expected two electron bands with nearly degenerate Fermi crossings (k_F) but different band bottom positions—a shallower one around -0.05 eV and a deeper one that extends to the top of the d_{xz}/d_{yz} holelike band at ~ -0.12 eV. The Luttinger volume of the two electron pockets gives $\sim 0.16\ e^-$/Fe. Considering that the C_4 symmetry of the crystal dictates the degeneracy between the d_{xz}/d_{yz} electron band bottom and corresponding d_{yz}/d_{xz} hole band top at X, the shallower electron band that is clearly not degenerate with the hole band is most likely of d_{xy} character, and the deeper one d_{xz} along Γ-X and d_{yz} along the perpendicular direction (see Supplemental Material [26]). This orbital character assignment seems to contradict the LDA prediction of the shallower electron band as d_{xz}/d_{yz} and the deeper one d_{xy} in FeSC [31], as observed in $Ba(Co_{0.07}Fe_{0.93})_2As_2$ [Figs. 1(f) and 1(g)]. However, this can be understood if we consider the KFS band structure as a whole. Three filled hole bands are observed near Γ [Figs. 1(d) and 1(e)], where the two lower ones can be identified as d_{xz}/d_{yz} and the higher one d_{xy} (see Supplemental Material [26]). Interestingly, the d_{xy} band is far more renormalized (a factor of ~ 10) compared to LDA than the d_{xz}/d_{yz} bands (a factor of ~ 3), indicating stronger correlation for the d_{xy} orbital. This is in sharp contrast to the $Ba(Co_{0.07}Fe_{0.93})_2As_2$ band structure, in which all orbitals are renormalized by about the same factor (~ 2) compared to LDA. Hence, our assignment of d_{xy} character to the shallower electron band is consistent with strong orbital-dependent renormalization, which brings the original deeper d_{xy} electron band at X to be shallower than the d_{xz}/d_{yz} band. This orbital-dependent renormalization behavior also emerges from our theoretical calculations as will be discussed later.

Next, an interesting phenomenon is observed with raised temperature. Figure 2(a) shows the electron bands at X under a polarization that has stronger matrix elements for d_{xy} than d_{xz} [32]. At low temperatures, d_{xy} band is clearly resolved with weaker intensity for the d_{xz} band. With increasing temperature, the spectral weight of the whole d_{xy} band noticeably diminishes, revealing the remaining d_{xz} band at high temperatures. In Fig. 2(b), the deeper d_{yz} band has more intensity than the corresponding d_{xz} band in Fig. 2(a), while the presence of the d_{xy} band is still very noticeable from the increased intensity near E_F where the two bands overlap, as well as from the energy distribution curves (EDCs) shown in Fig. 2(c). With increasing temperature, again, the spectral weight of the whole d_{xy} band diminishes, revealing the remaining d_{yz} band at high

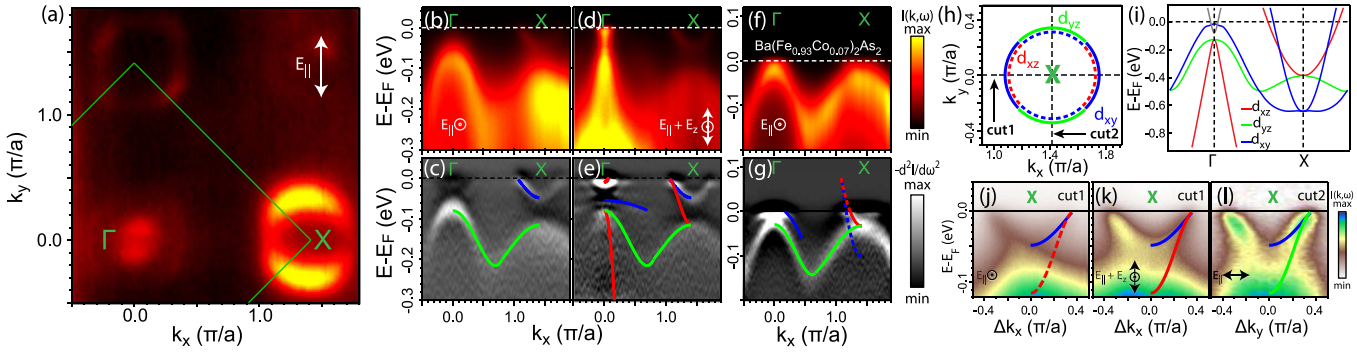

FIG. 1 (color online). Electronic structure of $K_xFe_{2-y}Se_2$. (a) FS mapping with the 2-Fe BZ boundary marked in green. (b), (d) Spectral images and (c), (e) second derivative in energy along the Γ-X direction. (f)–(g) Similar measurements as (b)–(c) on $Ba(Co_{0.07}Fe_{0.93})_2As_2$. (h) Schematic of the dominant orbital characters of the two electron pockets at X, with one pocket (dotted) imploded for clarity. (i) LDA calculations [30] for KFS. (j)–(l) Spectral images across X under different polarizations and cut directions. All light polarizations are marked. Dominant orbital characters indicated by color: blue (d_{xy}), red (d_{xz}), green (d_{yz}). All data taken at 30 K, with 47.5 eV photons except (d), (e), and (k), which were taken with 26 eV photons. We note very little k_z dispersion exists in the electron bands [27].

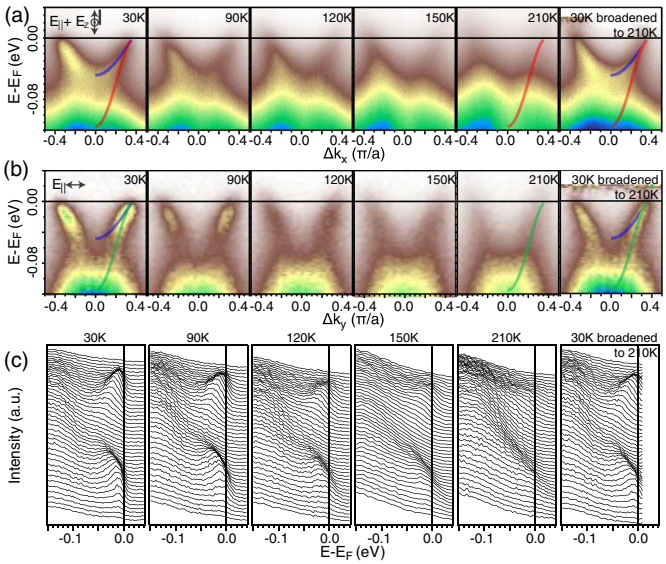

FIG. 2 (color online). Temperature dependence of electron bands at X. (a) Spectral images taken with 26 eV photons along cut1 as marked in Fig. 1(h). (b) Spectral images and (c) corresponding EDCs taken with 47.5 eV photons along cut2. Last column shows the 30 K data with an artificially introduced 210 K thermal broadening, in comparison to the real 210 K data.

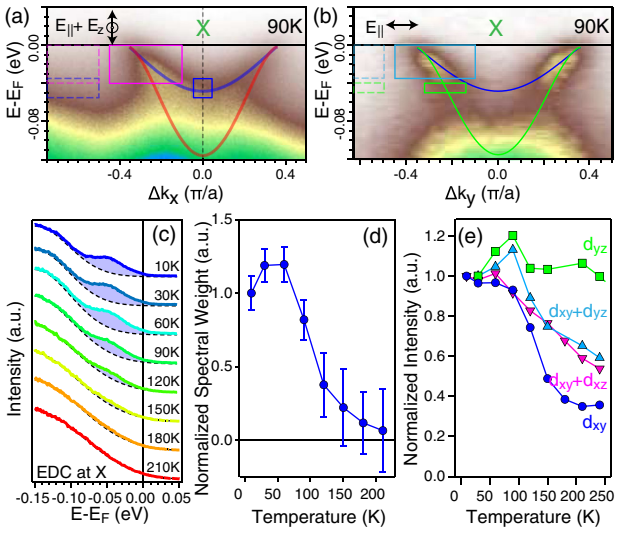

FIG. 3 (color online). Temperature dependence analysis. (a)–(b) 90 K spectral image of Fig. 2(a) and 2(b). (c) EDCs at X from (a) for selected temperatures, fitted to a Gaussian background (dotted line) and a Lorentzian peak (shaded region). (d) The integrated Lorentzian spectral weight is plotted against temperature. (e) Temperature dependence of the averaged intensity of the colored boxes in (a)–(b), with background (dotted box of the same energy window marked by same color) for each box subtracted. The resulting temperature-dependent curve is then normalized by the initial value. The blue (green) region has dominant spectral weight from the d_{xy} (d_{yz}) band, whereas the magenta (cyan) region is of mixed d_{xy} and d_{xz} (d_{yz}) characters.

temperatures, which clearly has a deeper band bottom than the shallower d_{xy} band. In addition, we have artificially introduced a 210 K thermal broadening to the 30 K spectra as shown in the last column of Fig. 2. The clear contrast to the 210 K data rules out a trivial thermal broadening as an origin for the observed diminishing of d_{xy} spectral weight.

To evaluate this behavior quantitatively, we analyze the temperature dependence of the EDCs at the X-point [Fig. 3(c)]. At all temperatures, there is a large hump background corresponding to the holelike dispersion at ~ -0.12 eV. At low temperatures, there is another peak around -0.05 eV corresponding to the d_{xy} band bottom. We fit these EDCs with a Gaussian for the hump background and a Lorentzian for the d_{xy} band. The integrated spectral weight for the fitted d_{xy} peak is plotted in Fig. 3(d), which decreases toward zero with increasing temperature, seen as a nontrivial drop between 100 and 200 K. As an independent check against trivial thermal effect, we choose small regions in the spectral image [marked in Figs. 3(a) and 3(b)] dominated by d_{xy} (blue), d_{yz} (green), mixed d_{xy}/d_{xz} (magenta), and mixed d_{xy}/d_{yz} (cyan) characters and plot their integrated intensities as a function of temperature [Fig. 3(e)]. The spectral weight from d_{xy}-dominated region rapidly decreases, consistent with the fitted result in Fig. 3(d), while that of d_{yz}-dominated region does not drop in a similar manner. The regions of mixed orbitals show a slower diminishing spectral weight compared to that for d_{xy}, reflecting the contributions from both d_{xz}/d_{yz} and d_{xy} orbitals. Although this method has the uncertainty of small leakage of other orbitals into the chosen regions, which is the likely cause of the finite residual value for the d_{xy} curve, the contrasting behavior of the d_{xy} versus d_{xz}/d_{yz} orbitals is clearly demonstrated. A temperature cycle test was performed to exclude the possibility of sample aging (see Supplemental Material [26]). Measurements on the sister compound RFS reveal similar behavior (Supplemental Material [26]), suggesting the generality of this phenomenon in this family of superconductors. This observation of a selected orbital that loses coherent spectral weight while the others remain metallic is reminiscent of a crossover into an OSMP in which selected orbitals become Mott localized while others remain metallic.

To further understand this phenomenon, we perform theoretical calculations based on a five-orbital Hubbard model to study the metal-to-insulator transition in the paramagnetic phase using a slave-spin mean-field method [33,34]. At commensurate electron filling $n = 6$ per Fe (corresponding to Fe^{2+} of the parent FeSC), we find the ground state of the system to be a metal, an OSMP, or a MI depending on the intraorbital repulsion U and the Hund's coupling J. Furthermore, the metal-to-insulator transition can be triggered by increasing temperature [Fig. 4(a)] due to the larger entropy of the insulating phase. At a fixed interaction strength [within a certain range, Fig. 4(a)], the system goes from a metal to an OSMP and then to a MI

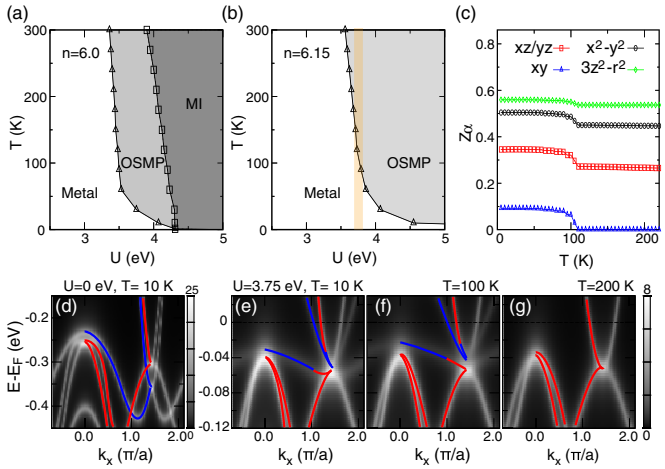

FIG. 4 (color online). Theoretical calculation based on a five-orbital Hubbard model. (a)–(b) Slave-spin mean-field phase diagrams of the five-orbital Hubbard model for KFS at $J/U = 0.15$ and two electron densities. OSMP and MI refer to orbital-selective Mott phase and Mott insulator, respectively. (c) The evolution of the orbital-resolved quasiparticle spectral weight Z_α with temperature at $n = 6.15$, $U = 3.75$ eV, and $J/U = 0.15$. (d)–(g) show the quasiparticle spectral functions along the Γ-X direction at $n = 6.15$. The color curves highlight the dominant orbital of the band, with d_{xz}/d_{yz} in red and d_{xy} in blue.

with increasing temperature. The MI phase is suppressed by electron doping. By contrast, the OSMP can survive, as shown in Fig. 4(b) for $n = 6.15$, which roughly corresponds to the filling of the superconducting state from ARPES measurements. From the evolution of the orbitally resolved quasiparticle spectral weight, Z_α, as a function of the temperature [Fig. 4(c)], we show that the OSMP corresponds to the d_{xy} orbital being Mott localized ($Z = 0$) and the rest of the $3d$ orbitals remaining delocalized ($Z > 0$). This result originates primarily from a combined effect of the orbital dependence of the projected density of states and the interplay between the Hund's coupling and crystal level splitting (see Supplemental Material [26] and Ref. [35]).

To compare with the ARPES data, we have calculated the quasiparticle spectral function $A(k, E)$ in the 2-Fe BZ. At low temperature and in the noninteracting limit $U = 0$ [Fig. 4(d)], the electronic structure of the model agrees well with that of LDA, with the d_{xy} band deeper than the d_{xz}/d_{yz} band at X. This order switches with sufficiently strong interaction. At $U = 3.75$ eV [Fig. 4(e)], the d_{xy}-dominated bands are pushed above their d_{xz}/d_{yz} counterparts by the strongly orbital-dependent mass renormalization, as reflected in the orbital-dependent quasiparticle spectral weights [Fig. 4(c)]. The mass renormalization is the largest for the d_{xy} orbital (~ 10) and smaller for the d_{xz}/d_{yz} orbitals (~ 3), which is compatible with the low-temperature ARPES results [Fig. 1(e)]. The temperature-induced crossover to the OSMP is clearly seen from the complete suppression of the spectral weights in the d_{xy} orbital that accompanies the moderate reduction of the weights in other orbitals [Figs. 4(c) and 4(e)–4(g), in agreement with the ARPES results (Figs. 2 and 3).

The temperature-induced nature of the crossover constrains these AFS superconductors to be very close to the boundary of the OSMP in the zero temperature ground state, which is also the superconducting state. The best agreement between theory and experiments is achieved at $U \sim 3.75$ eV. While the absolute value of this interaction is sensitive to the parametrization of the crystal levels and Hund's coupling, it is instructive to make a qualitative comparison with the case of the iron pnictides. The enhanced correlation effects for AFS tracks the reduction of the width of the ($U = 0$) d_{xy} band, which is about 0.7 of its counterpart in 1111 iron arsenides.

One known concern for the AFS materials is the existence of mesoscopic phase separation into superconducting and insulating regions [36], which would both contribute spectral intensity in ARPES data. From measurement on an insulating RFS sample (Supplemental Material Fig. S5(d) [26]), we see negligible spectral weight and no well-defined dispersions within 0.1 eV of E_F, as expected for an insulator. Hence, the insulating regions in the superconducting compounds do not contribute spectral weight to the near-E_F energy range, in which the temperature-induced crossover is observed. In addition, superconducting gap consistent with previous reports [27,29] is observed to open below T_C on the electron bands (see Supplemental Material [26]), confirming the origin of these observed bands to the superconducting regions of the sample. We have also measured a KFS sample whose resistivity is intermediate between superconducting and insulating (Supplemental Material Fig. S5(b) [26]), and was previously proposed to be semiconducting containing both metallic and insulating phases [37]. Interestingly, its d_{xz}/d_{yz} bands, which must come from the metallic phase, appear further renormalized by a factor of 1.3 compared with those of the superconducting compounds. In addition, we resolve small but finite spectral weight for a very shallow d_{xy} electron band near the X-point (Supplemental Material Fig. S6(c) [26]). As expected, the peak position is even closer to E_F compared with superconducting samples, consistent with further renormalization for the shallower d_{xy} band near X, which is harder to discern with temperature dependent study. These observations are consistent with the OSMP picture in that the metallic phase in this intermediate doping compound is likely even closer to the boundary of OSMP at low temperatures from the mass-diverging behavior of the d_{xy} bands. For the same interaction strength, calculation from our model also identifies the low-temperature ground state of the superconducting, intermediate, and insulating phases to be located close to an OSMP, just at the boundary of an OSMP, and in a MI phase, respectively (see Supplemental Material [26]).

While we cannot completely rule out alternative explanations for the observations presented above (see Supplemental Material [26]), the consistency of the totality of the observations—including strongly orbital dependent-band renormalization for d_{xy} versus d_{xz}/d_{yz} at both Γ and X in the low-temperature metallic state, the nontrivial temperature-dependent spectral weight depletion for only the d_{xy} band, systematic doping dependence of the related effects in the intermediate and insulating compounds—and the theoretical calculations make this understanding a most likely scenario, suggesting that the superconductivity in this AFS family exists in close proximity to Mott behavior.

We thank V. Brouet, W. Ku, B. Moritz, and I. Mazin for helpful discussions. ARPES experiments were performed at the Stanford Synchrotron Radiation Lightsource and the Advanced Light Source, which are both operated by the Office of Basic Energy Science, U.S. DOE. The work at Stanford is supported by DOE Office of Basic Energy Science, Division of Materials Science and Engineering, under Contract No. DE-AC02-76SF00515. The work at Rice has been supported by NSF Grant No. DMR-1006985 and the Robert A. Welch Foundation Grant No. C-1411. The work at Houston is supported in part by US Air Force Office of Scientific Research Contract No. FA9550-09-1-0656 and the state of Texas through the Texas Center for Superconductivity at the University of Houston. MY thanks to the NSF Graduate Research Fellowship Program for financial support.

[1] P. A. Lee, N. Nagaosa, and X.-G. Wen, Rev. Mod. Phys. **78**, 17 (2006).
[2] D. H. Lu *et al.*, Nature (London) **455**, 81 (2008).
[3] W. L. Yang *et al.*, Phys. Rev. B **80**, 014508 (2009).
[4] M. M. Qazilbash, J. J. Hamlin, R. E. Baumbach, L. Zhang, D. J. Singh, M. B. Maple, and D. N. Basov, Nat. Phys. **5**, 647 (2009).
[5] Z. P. Yin, K. Haule, and G. Kotliar, Nat. Mater. **10**, 932 (2011).
[6] A. Tamai *et al.*, Phys. Rev. Lett. **104**, 097002 (2010).
[7] Y. Lubashevsky, E. Lahoud, K. Chashka, D. Podolsky, and A. Kanigel, Nat. Phys. **8**, 309 (2012).
[8] Z. K. Liu *et al.*, Phys. Rev. Lett. **110**, 037003 (2013).
[9] T. J. Liu *et al.*, Nat. Mater. **9**, 718 (2010).
[10] J. Guo, S. Jin, G. Wang, S. Wang, K. Zhu, T. Zhou, M. He, and X. Chen, Phys. Rev. B **82**, 180520 (2010).
[11] A. Krzton-Maziopa, Z. Shermadini, E. Pomjakushina, V. Pomjakushin, M. Bendele, A. Amato, R. Khasanov, H. Luetkens, and K. Conder, J. Phys. Condens. Matter **23**, 052203 (2011).
[12] C.-H. Li, B. Shen, F. Han, X. Zhu, and H.-H. Wen, Phys. Rev. B **83**, 184521 (2011).
[13] M.-H. Fang, H.-D. Wang, C.-H. Dong, Z.-J. Li, C.-M. Feng, J. Chen, and H. Q. Yuan, Europhys. Lett. **94**, 27009 (2011).
[14] H.-D. Wang, C.-H. Dong, Z.-J. Li, Q.-H. Mao, S.-S. Zhu, C.-M. Feng, H. Q. Yuan, and M.-H. Fang, Europhys. Lett. **93**, 47004 (2011).
[15] W. Bao, Q.-Z. Huang, G.-F. Chen, D.-M. Wang, J.-B. He, and Y.-M. Qiu, Chin. Phys. Lett. **28**, 086104 (2011).
[16] Q. Si and E. Abrahams, Phys. Rev. Lett. **101**, 076401 (2008).
[17] R. Yu, J.-X. Zhu, and Q. Si, Phys. Rev. Lett. **106**, 186401 (2011).
[18] Y. Zhou, D.-H. Xu, F.-C. Zhang, and W.-Q. Chen, Europhys. Lett. **95**, 17003 (2011).
[19] R. Yu and Q. Si, Phys. Rev. B **84**, 235115 (2011).
[20] L. Craco, M. S. Laad, and S. Leoni, Phys. Rev. B **84**, 224520 (2011).
[21] M. Neupane, P. Richard, Z.-H. Pan, Y.-M. Xu, R. Jin, D. Mandrus, X. Dai, Z. Fang, Z. Wang, and H. Ding, Phys. Rev. Lett. **103**, 097001 (2009).
[22] V. I. Anisimov, I. A. Nekrasov, D. E. Kondakov, T. M. Rice, and M. Sigrist, Eur. Phys. J. B **25**, 191 (2002).
[23] L. de' Medici, S. R. Hassan, M. Capone, and X. Dai, Phys. Rev. Lett. **102**, 126401 (2009).
[24] Y.-Z. You, F. Yang, S.-P. Kou, and Z.-Y. Weng, Phys. Rev. B **84**, 054527 (2011).
[25] S. J. Moon *et al.*, Phys. Rev. B **81**, 205114 (2010).
[26] See Supplemental Material at http://link.aps.org/supplemental/10.1103/PhysRevLett.110.067003 for discussions of orbital assignment, observation of superconducting gap, temperature cycle test, results on RFS, details of the five-orbital Hubbard model, and doping dependence.
[27] Y. Zhang *et al.*, Nat. Mater. **10**, 273 (2011).
[28] T. Qian *et al.*, Phys. Rev. Lett. **106**, 187001 (2011).
[29] D. Mou *et al.*, Phys. Rev. Lett. **106**, 107001 (2011).
[30] I. A. Nekrasov and M. V. Sadovskii, JETP Lett. **93**, 166 (2011).
[31] S. Graser, A. F. Kemper, T. A. Maier, H.-P. Cheng, P. J. Hirschfeld, and D. J. Scalapino, Phys. Rev. B **81**, 214503 (2010).
[32] M. Yi *et al.*, Proc. Natl. Acad. Sci. U.S.A. **108**, 6878 (2011).
[33] R. Yu and Q. Si, Phys. Rev. B **86**, 085104 (2012).
[34] L. de'Medici, A. Georges, and S. Biermann, Phys. Rev. B **72**, 205124 (2005).
[35] R. Yu and Q. Si, arXiv:1208.5547.
[36] W. Li *et al.*, Nat. Phys. **8**, 126 (2012).
[37] F. Chen *et al.*, Phys. Rev. X **1**, 021020 (2011).